JAAS

PAPER

Cite this: *J. Anal. At. Spectrom.*, 2019, **34**, 1892

Microwave-assisted laser induced breakdown molecular spectroscopy: quantitative chlorine detection

M. A. Wakil and Zeyad T. Alwahabi *

Received 26th April 2019
Accepted 9th July 2019

DOI: 10.1039/c9ja00151d

rsc.li/jaas

Quantitative detection of chlorine, through molecular emission from CaCl, using microwave assisted laser induced breakdown spectroscopy (MW-LIBS) has been demonstrated. CaCl emission is utilised in the spectral range of 617.9–621.5 nm. Using time-resolved emission spectra of CaCl at 617.9 nm, following a 1.5 ms microwave pulse, an optimum gate-width and gate-delay have been established. A linear relationship between the intensity of CaCl molecular emission and chlorine concentration on a cement surface has been validated. This yields a limit of detection (LoD) of 47 ± 7 μg g^{-1} and ~170 ± 59 μg g^{-1} for chlorine, based on 100 shots averaged and a single shot, respectively. The results represent a 10-fold improvement in the chlorine LoD on cement.

1. Introduction

The detection of chlorine is important in process industries because chlorine acts as an active corrosive agent in concrete structures. Harmful species such as chlorides may penetrate together with water through the capillary pore space, which may trigger different damaging processes.[1] The major destructive processes are the corrosion of reinforcement especially pitting corrosion and concrete corrosion.[2] More specifically, chlorine can play a role in the process of stress corrosion cracking of dry cask storage located in marine environments[3] as well as in partial melting of the Martian mantle.[4] Moreover, chlorine acts as a catalyst for pitting corrosion in steel in the presence of water and O_2.[5] On the other hand, chlorine acts as an essential element in chemical building blocks, food, water purification, medicines, advanced technological devices, air conditioning refrigerants, paints, energy efficient windows, *etc.* Despite that, insufficient disinfection of chlorine can cause many hazards, and adversely high concentrations lead to toxicity in human beings and animals.[6] For damage assessment of reinforced concrete and steel, this harmful species, which is chlorine, needs to be determined properly. The detection of chlorine is important for monitoring free chlorine in real life usage as mentioned above. It is also important for complete understanding of early Mars and the presence of water in Mars.[7]

Laser Induced Breakdown Spectroscopy (LIBS) is considered as a well-established laser-ablation based analysis technique due to its distinguishing characteristics, one being the ability to perform chemical analysis on any solid sample directly. Although LIBS is advantageous due to its unique features such as the lack of need for sample preparation, speed, ease of handling and that it is almost as non-destructive as methods reported in the literature,[8–10] it is found to be less sensitive to elements (such as those present in nuclear fuel) which have a complex structure,[11] low excitation efficiency[12] and high ionization energy[13] such as halogens. It is reported that halogens such as chlorine produce weak emission making them more difficult to characterise compared to elements with prominent peaks such as alkalis, alkaline earth elements and transition metals.[13,14] Detection limits for halogens are less than satisfactory for demanding applications. Direct detection of chlorine based on atomic emission is difficult because the resonance lines of Cl I belong to the deep VUV at 134–140 nm, corresponding to ^4P and 4^2P, which have very high excitation energy and are difficult to populate. It is worth noting that chlorine may also be detected near 754 nm and 837 nm; however these transitions originate from states at very high excitation energies, which are 85 735 cm^{-1} and 83 894 cm^{-1}.

One possible alternative to direct measurement of chlorine is to use the detection of alkali metals as a surrogate to deduce the presence of salts that have chlorine (Cl), assuming that the concentration of these metals is proportional to that of Cl,[3,15] but in this case, homogeneous salt deposition is also essential. Another prospective alternative for chlorine detection is to use molecular emission because the molecular structure has a strong influence on the final emission pattern.[16] It has been shown that by using molecular emission, the sensitivity of LIBS for chlorine can be significantly improved due to the simple molecules that form in the plasma.[7,13] Haisch *et al.* have shown that the detection limit for chlorine can be significantly enhanced using molecular emission bands.[17]

De Giacomo *et al.* concluded that there are three conditions need to be satisfied for a molecular emission bands to be

School of Chemical Engineering, The University of Adelaide, SA 5005, Australia. E-mail: zeyad.alwahabi@adelaide.edu.au

observed. These are: an appropriate plasma temperature, a sufficient reactants density and an observable molecular transition.[18] In accordance with that, since the past few years molecular LIBS is becoming an exciting area of study for proper characterisation of chlorine. Haisch *et al.* reported CuCl molecular emission at 440 nm.[17] Álvarez *et al.* observed CaF emission at around 535 nm (ref. 19) and reported the limit of detection for fluorine at about 50 μg g^{-1}. Yao *et al.* used CN molecular emission at 388.34 nm for analysing fly ash.[20] Rezaei *et al.* analysed the aluminium percentage in plastic bonded explosives using AlO and CN molecular bands.[21] Guo *et al.* determined boron using a BO molecular band at 255.14 nm.[22] However, few studies have been undertaken for molecular chlorine in spite of its importance mentioned above. Earlier studies used different alkali elements for successful chlorine (Cl) molecular emission. Haisch *et al.* considered CuCl and reported a ten-fold improvement in the detection limit for Cl but they did not mention the detection limit.[17] Bhatt *et al.* used SrCl and SrO emissions for determining Sr concentration.[23] They reported that the detection limit using molecular emission is worse than that using atomic emission. Vogt *et al.* examined two different alkali elements for Cl detection, namely MgCl and CaCl.[7] They reported that the MgCl molecular band is unclear with LIBS while CaCl is more sensitive for Cl detection. Gaft *et al.* detected Cl in a mixture of 0.4% $CaCl_2$ using a CaCl molecular emission band.[24] Vogt *et al.* suggested in their study that calcium-free salt is not suitable for detecting Cl *via* CaCl.[25] Alvarez-Llamas *et al.* used 100 mJ laser energy for fluorine detection using Ca free samples following CaF emission.[12] Bhatt *et al.* succeeded with a laser energy of 82 mJ to calculate the LoD for Sr in a mixture of $SrCl_2$ and Al_2O_3, following SrCl and SrO molecular emissions.[23] Guo *et al.* applied 60 mJ laser energy on a solid matrix mixture of H_3BO_3 and $C_6H_{12}O_6 \cdot H_2O$ and observed BO molecular emission.[22] In addition, Rezaei *et al.* observed AlO emission using 100 mJ laser energy on aluminized PBX samples.[21]

CaCl possesses relatively strong emission bands ($A^2\Pi \rightarrow X^2\Sigma$, $B^2\Sigma \rightarrow X^2\Sigma$) at 593.5, 606.8, 617.9, 620.5 and 631.4 nm,[26] making it suitable for low level Cl detection.[2,9]

MW-LIBS is a popular method in which low laser energy is sufficient for elemental detection instead of high laser energy for LIBS to improve the LoD. MW-LIBS offers several benefits such as long plasma lifetime, larger volume, strong emission intensity, stability with time and the ability to reduce self-absorption[27–30] A laser-assisted microwave plasma spectroscopy (LAMPS) system was reported based on the electric field to the laser induced plasma by the enclosed MW cavity.[31] This extends the plasma lifetime resulting in a promising improvement in sensitivity. The LAMPS technique was also reported by Efthimion,[32] with the achievement of ~200 times enhancement. Liu *et al.* applied a MW cavity system to examine ceramics and soil samples. They demonstrated an enhancement factor of ~33 for sodium detection.[33,34] In gaseous samples, Ikeda *et al.* used an antenna to study the characteristics of laser and spark induced plasmas where a 15 times enhancement for Pb was reported.[27] Antenna-coupled MW enhanced LIBS on solid samples was also introduced by Khumaeni *et al.* at low-pressure in enclosed cavity environments.[11,35] A loop antenna was used to deliver MW radiation and a 32 times enhancement of Gd lines was observed. Tampo *et al.* achieved a 50-fold enhancement of Gd lines at a low pressure of 0.6 kPa.[36] Viljanen *et al.* observed an approximately 93-fold higher LoD with MW-LIBS for copper using solid samples.[30] Wall *et al.* reported an 11.5-fold improved LoD for indium in a water solution.[37] MW-LIBS has been demonstrated for gas samples for the detection of Na, K and Ca in flames.[38] Furthermore, Iqbal demonstrated MW-LIBS with spectrometer free detection of indium, based on imaging.[39]

MW-LIBS offers extension of the lifetime of the laser induced plasma. This is usually followed by a relatively longer detection gate (~500 μs). A longer plasma lifetime along with a prolonged detection gate provides some difficulties because emission from molecules and radicals become stronger, blocking a large atomic spectral range. However, when the process of molecular formation and emission is carefully used, the process can benefit the detection of a few elements such as chlorine. This paper reports the application of MW-LIBS directed towards quantitative detection of Cl *via* CaCl ($A^2\Pi \rightarrow X^2\Sigma$) emission at 617.9 nm and 620.5 nm.

2. Materials and methods

2.1 MW-LIBS setup

The experimental setup of MW-LIBS used for this work is presented schematically in Fig. 1. A second harmonic from a Q-switch Nd:YAG laser, Quantel (Brilliant B), ~6 ns with a repetition of 10 Hz was used. The pulse energy was controlled using a half-wave plate (HWP) and Glan-laser polariser (P). The laser energy was measured with a Pyroelectric sensor (Thorlabs, ES 220C). The beam was focussed onto the sample surface using a fused silica lens with $f = 100$ mm. The spot size obtained at the focal point was estimated to be 140 μm^2 while the propagation of the laser beam was at an angle of 15° to the vertical. A 7.5 mJ laser energy was considered where 3.5–10 mJ laser energy was analysed for enhancement calculation. To achieve the ablation from the fresh sample surface for each shot, the sample was placed on a rotating disk with an angular velocity of 7 rotations per minute. A second CW laser, with a camera, was used to monitor the exact distance between the sample surface and the fused silica lens.

A water cooled pulsed-microwave system operated at 2.45 GHz (Seirem), shown in Fig. 1, was used. The microwave radiation was directed *via* a WR340 waveguide to a 3-stub impedance tuner and then to a waveguide-to-coaxial adaptor (WR340RN) through a quartz window. The waveguide-to-coaxial adaptor was connected to a 1 m flexible coaxial cable (50 Ω NN cable) with 0.14 dB @ 2.45 GHz. A semi-rigid cable (RG402/U) was then connected at the end of the coaxial cable. The other end of the semi-rigid cable was attached to a Near Field Applicator (NFA) as shown in ref. 30 and 40. The NFA was located about 1 mm above the sample surface and 0.5 mm horizontally away from the ablation spot. The microwave pulse duration and power were controlled with an analogue signal pulse generator (Aim-TTi).

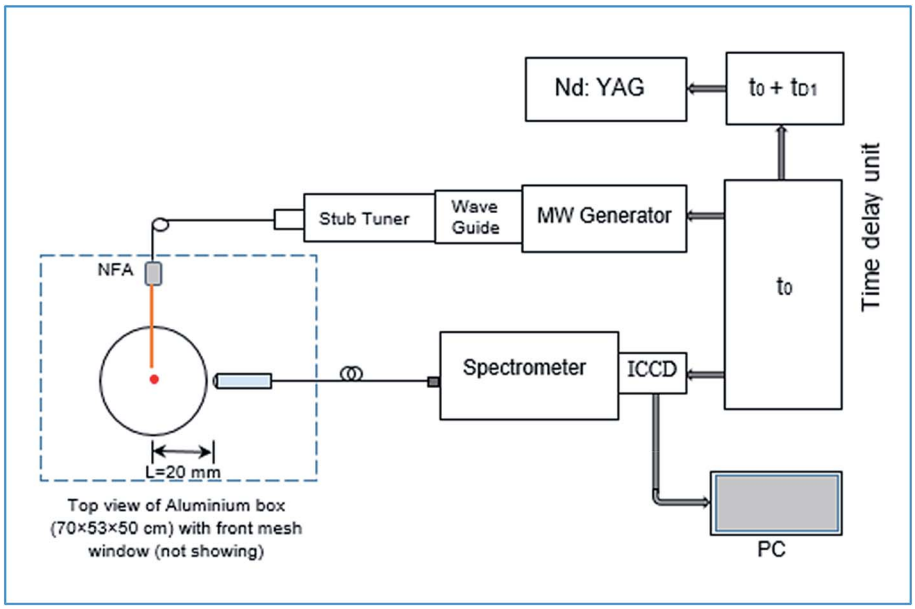

Fig. 1 Schematic diagram of the MW-LIBS setup.

For the spectroscopic detection, the plasma emission was collected directly using a bifurcated fibre bundle (Thorlabs, BFY400HS02). The fibre bundle has a core size of 400 μm and a transmission range of 250–1200 nm. The optical line, the sample holder, the NFA and one end of the fibre were placed inside an aluminium box to minimise the residual microwave radiation, as shown in Fig. 1. One side of the aluminium box was covered with metal mesh acting as an observation window.

The spectrometer (Andor Shamrock 500i) with a grating of 2400 lines per mm has a spectral resolving power of 10 000, and the spectral resolution is 0.031 nm in the spectral range of 320–332 nm. The attainable wavelength range for the spectrometer, with a holographic grating, is 200–705 nm. An intensified CCD camera (Andor, iStar) was utilized to record the spectral signal, and it was synchronised with the laser and the microwave generator. For each concentration, 100 single shots were recorded and averaged. The experiment was conducted in the atmospheric environment.

2.2 Samples

To assess the linearity in the calibration curve and the detection of chlorine (Cl), several calibration samples with different Cl concentrations were prepared by wet impregnation from cement and KCl. The KCl anhydrous (Sigma Aldrich) powder with different weights of 6.75–82.8 mg, considering the weight of Cl in KCl, was mixed with distilled water to make a solution.

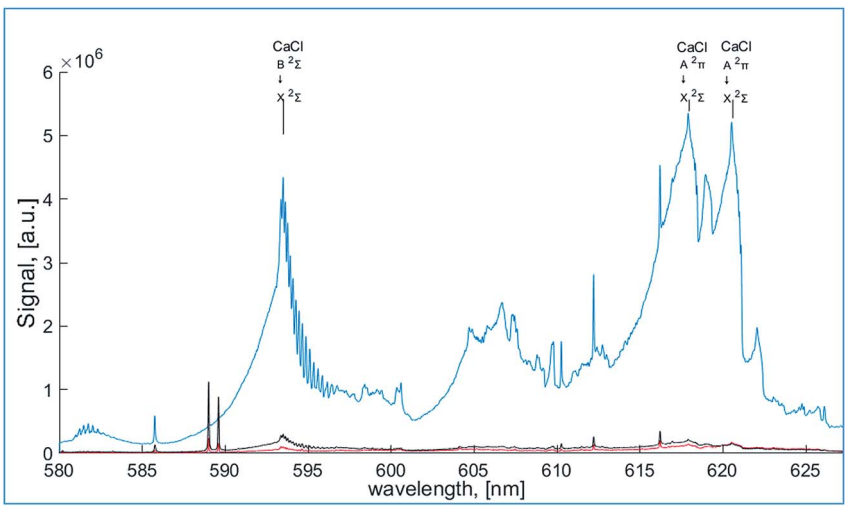

Fig. 2 MW-LIBS spectra of pure $CaCl_2$ (blue), $CaSO_4$ + KCl (2.07% Cl) (black), and cement + KCl (2.07% Cl) (red). The spectra were recorded using 7.5 mJ laser energy, 600 W microwave power, 500 ns gate-delay, 300 μs gate-width and an accumulation of 100 shots.

Each solution was mixed with an exact amount of cement (4 g) with an uncertainty of ±0.00033 g to make a paste, for all samples. Eleven samples were prepared with varying Cl concentrations from 0.08 to 2.07% (by weight). The paste was placed in a circular disk to make a pellet and dried with a dryer.

3. Results and discussion

3.1 Spectral information and enhancement

Typical spectra of molecular CaCl recorded in LIBS with microwave radiation are presented in Fig. 2. A MW-LIBS scan in the range of 580–630 nm was analysed to identify the best spectral range of CaCl required for the calibration. Four possible emission spectra of CaCl in this range, *i.e.*, 593.5 nm, 606.4 nm, 617.9 nm and 620.5 nm, as shown in Fig. 2 were identified. The MW-LIBS scan was done with three different sample sources. Samples made of pure $CaCl_2$ (Sigma Aldrich, 98% purity) were also tested for the confirmation of the absolute CaCl spectral range. The formation of CaCl molecular spectra depends largely on the calcium-based matrix.[25] Cement was used as a base material of calcium because of the large percentage of calcium in cement (~40% in Portland cement). The second reason for using cement as a base material for chlorine detection is corrosion related issues, such as pitting corrosion and concrete corrosion, in the concrete by chlorine. Fig. 3 also confirmed the presence of calcium with sufficiently high signals of calcium at 610.27 nm, 612.22 nm and 616.217 nm. Among all the possible emission spectra of CaCl, those at 617.9 nm and 620.5 nm were considered for the calibration curve because the spectral wavelength range had higher enhancement than in the range of 593.5 nm as shown in Fig. 4(a and b). Furthermore, it was observed that using MW-LIBS, there is another spectral feature near 593.5 nm that interferes with CaCl emission.

The spectral range of 616–625 nm was used to develop the calibration curve for Cl detection. This spectral range presents

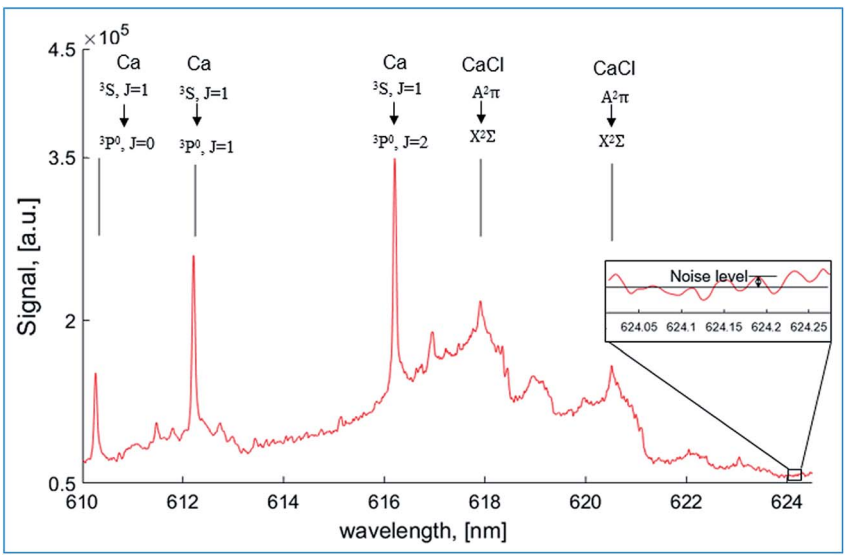

Fig. 3 MW-LIBS spectra of cement + KCl (2.07% Cl) at 7.5 mJ laser energy, 600 W microwave power, 500 ns gate-delay, 300 μs gate-width and an accumulation of 100 shots.

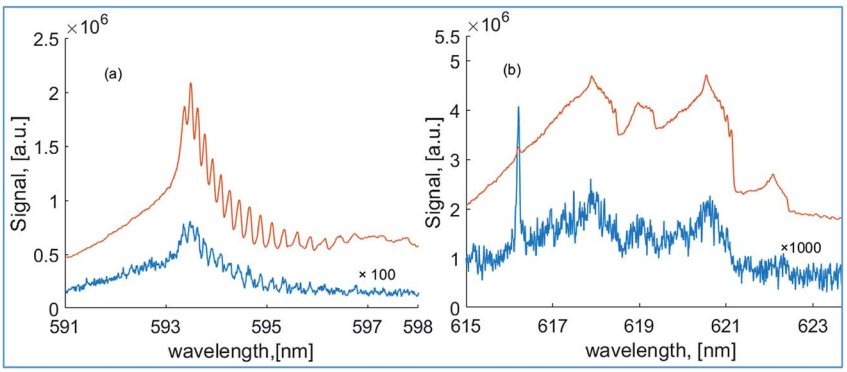

Fig. 4 Typical pure $CaCl_2$ spectra recoded at two spectral ranges (591–598 nm (a) and 615–623.5 nm (b)), with 600 W microwave power (red), and without microwave (blue), at 7.5 mJ laser energy, 500 ns gate-delay, and 300 μs gate-width. For clarity, the LIBS signal (blue) was multiplied by a factor of 100 and 1000 for spectral ranges (a) and (b), respectively.

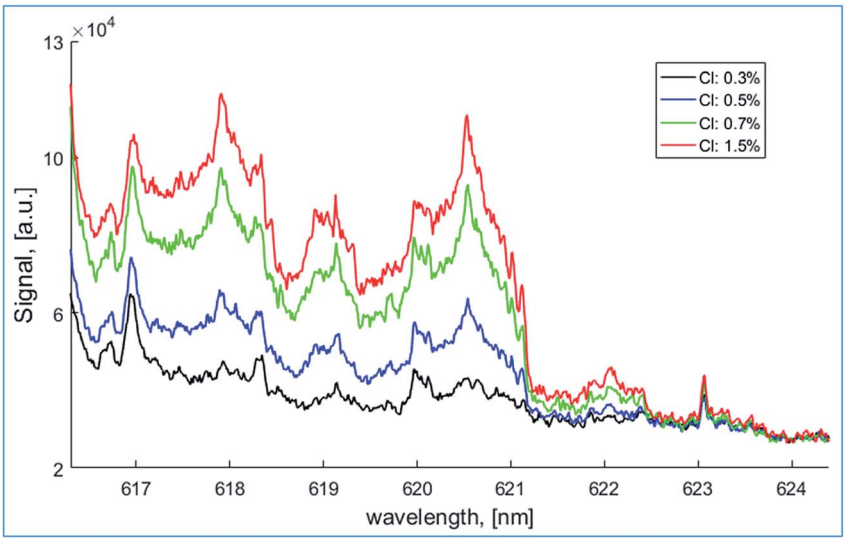

Fig. 5 MW-LIBS spectra for different chlorine concentrations at 7.5 mJ laser energy, 600 W microwave power, 500 ns gate-delay, 300 μs gate-width and an accumulation of 100 shots.

a suitable emission spectrum with minimum background noise. Fig. 5 shows the sample emission spectrum of CaCl for different concentrations of Cl using MW-LIBS.

3.2 Temporal evolution of MW-LIBS signal measurements

The temporal evolution of molecular emission intensity was investigated for MW-LIBS by maintaining a constant gate width of 300 μs and varying the gate delay from 0 ns to 2 μs. The temporal evolution of MW-LIBS is shown in Fig. 6. It was observed that the CaCl signal had an interference with the CaO signal at around 615 nm (ref. 24) shown in Fig. 6(a). A 300 μs gate width was found optimum to maximise the CaCl signal. Fig. 6(a) shows that the formation of the two radicals CaCl and CaO differs with respect to time. It was seen that the CaO signal was high initially and decreased with time until 1000 ns and increased again. Because of the constant amount of Ca present, the CaO signal was dominant initially and then the CaCl signal became stronger. To be able to investigate the optimum gate-delay, the intensities I_{CaCl} and I_{CaO} were first normalised to obtain $I_{\mathrm{CaCl}}^{\mathrm{norml}}$ and $I_{\mathrm{CaO}}^{\mathrm{norml}}$, respectively. The difference between the two normalised quantities ($I_{\mathrm{CaCl}}^{\mathrm{norml}} - I_{\mathrm{CaO}}^{\mathrm{norml}}$) was then plotted *versus* time, as shown in Fig. 6(b). Fig. 6(b) shows clearly that the quantity ($I_{\mathrm{CaCl}}^{\mathrm{norml}} - I_{\mathrm{CaO}}^{\mathrm{norml}}$) starts increasing at a gate-delay of 500 ns. Therefore, a gate-delay and gate-width of 500 ns and 300 μs, respectively, were used for CaCl detection.

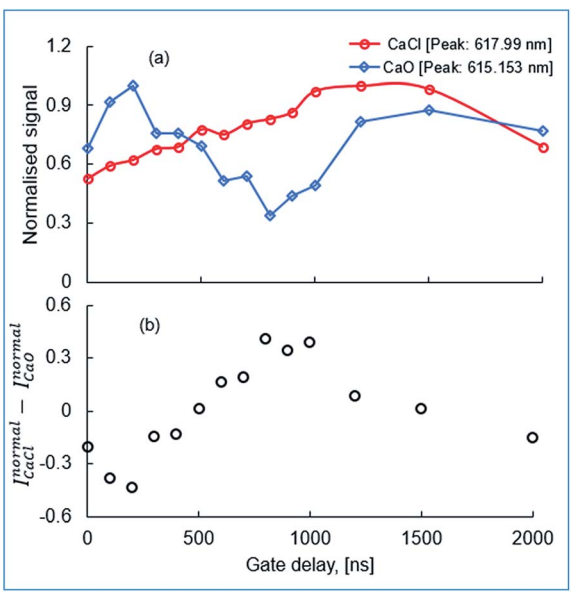

Fig. 6 Temporal evolution of the normalised MW-LIBS signal of CaO and CaCl (a) and the normalised signal difference ($I_{\mathrm{CaCl}}^{\mathrm{norml}} - I_{\mathrm{CaO}}^{\mathrm{norml}}$) (b) recoded on the sample with 1% Cl using 7.5 mJ laser energy and 600 W microwave power.

3.3 Dependence of microwave power on experimental parameters

The dependence of the MW-LIBS signal intensity on MW power at different laser energies was investigated, with the aim of optimising the MW-LIBS signal. Fig. 7(a) shows the effect of signal to noise ratio (SNR) on microwave power. The noise level was obtained in the range of 624.01 nm to 624.23 nm, as shown in the typical inset presented in Fig. 3. As shown in Fig. 7(a), the signal to noise ratio with MW-LIBS is higher than in LIBS. This is due to the signal enhancing ability of the microwave system. The external energy supplied, using microwave radiation, will sustain the free electrons present within the laser-induced plasma. These reenergized free electrons act as an excitation source, *via* collisional processes, leading to lifetime extension which finally leads to signal enhancement.[33,37] It is seen from Fig. 7(a) that the increase in microwave power did not increase the signal to noise ratio significantly because the increase in microwave power caused a higher noise level. Chen *et al.*[40] demonstrated the same behaviour of microwave power on the

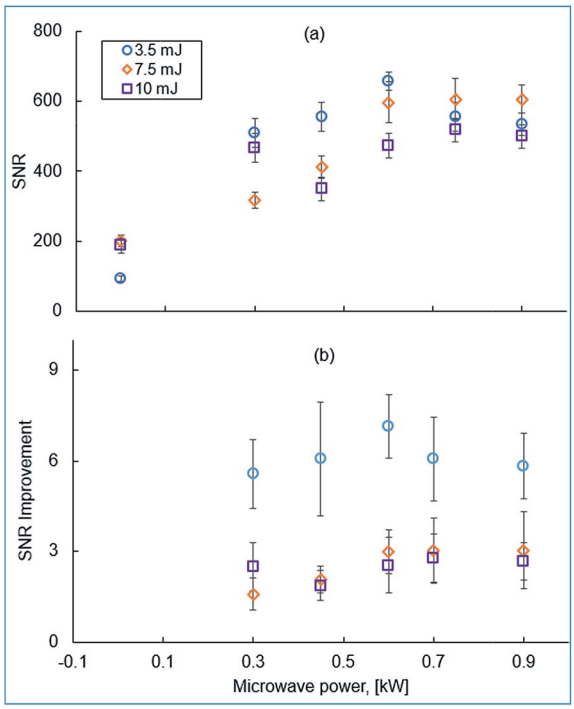

Fig. 7 (a) Signal to noise ratio (SNR) (a) and SNR improvement (b) of MW-LIBS of 2.07% Cl content samples recorded at 500 ns gate-delay, 300 μs gate-width and an accumulation of 100 shots.

SNR. It was observed from Fig. 7(a) that the increase of microwave power after 0.6 kW did not help to increase the SNR. For proper selection of microwave power for the detection of Cl, SNR improvement calculation was done as shown in Fig. 7(b). As Fig. 7(b) shows, 0.6 kW microwave power maximises the SNR improvement. Fig. 7(b) shows that the low laser energy (3.5 mJ) provides relatively higher enhancement than high laser energy (7.5 mJ or 10 mJ). This is due to the ease of microwave coupling at a lower laser energy. Increasing the laser energy will result in an increase in the electron density of the plasma's core which will result in a reduction of microwaves that penetrate into the plasma resulting in a measurement similar to that of a conventional LIBS.[30,37] It was found experimentally that by using 7.5 mJ laser energy, a reasonable MW-LIBS signal was possible even with low values of Cl concentration. Using 600 W microwave power, the chlorine SNR improved 2.5-fold, with respect to LIBS only. It is worth noting that the LIBS signal may be increased by using high laser energy. However, it is advantageous to use low laser energy to prevent sample damage and provide a practical pathway for mobile devices.

3.4 Quantitative detection of chlorine

The LoD of Cl using atomic lines reported by Wilsch *et al.* is 0.15% in concrete cores.[41] Burakov *et al.* found an LoD of 0.05% in cement based materials.[42] Weritz *et al.* analysed different building materials and reported the LoD of Cl at about 0.5%.[43] Gehlen *et al.* used UV lines of Cl (134.72 nm) and calculated 0.1% LoD from concrete.[44] For quantitative detection of Cl, molecular emission was considered rather than atomic lines. Calibration curves were determined with LIBS and MW-LIBS molecular signals of CaCl. For correct calibration, a Cl free sample was first investigated as shown in Fig. 8.

For developing the calibration curve, the experimental parameters were 7.5 mJ laser energy, 0.6 kW microwave power, 500 ns gate delay, 300 μs gate width and a microwave pulse duration of 1.5 ms. Fig. 9 and 10 show the calibration curve with LIBS and MW-LIBS for 100 shot accumulation and single shot simultaneously.

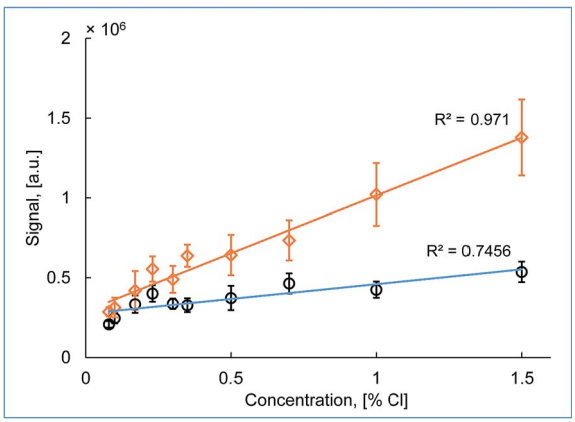

Fig. 9 Calibration curve of [Cl] with LIBS (blue) and MW-LIBS (red) at 7.5 mJ laser energy, 600 W microwave power, 500 ns gate-delay and 300 μs gate-width with an accumulation of 100 shots. The slope of the fitting is 724 466 and 185 593 for LIBS and MW-LIBS, respectively.

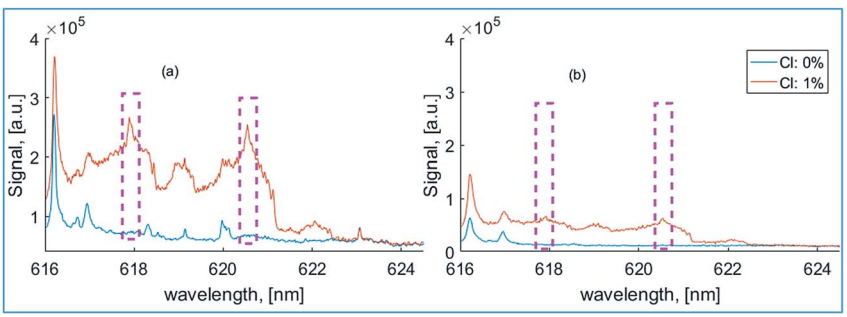

Fig. 8 MW-LIBS (a) and LIBS (b) spectra for Cl free and Cl containing samples at 7.5 mJ laser energy, 600 W microwave power, 500 ns gate-delay, and 300 μs gate-width with an accumulation of 100 shots.

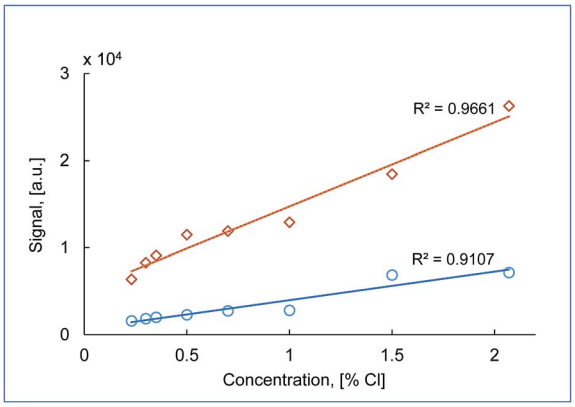

Fig. 10 Calibration curve of [Cl] with LIBS (blue) and MW-LIBS (red) at 7.5 mJ laser energy, 600 W microwave power, 500 ns gate-delay and 300 μs gate-width for one single shot. The slope of the fitting is 9651.7 and 3289.6 for LIBS and MW-LIBS, respectively.

Table 1 LoD reported in the literature

Method	Matrix	LoD	Reference
LIBS	Concrete core	0.15%	41
LIBS	Cement	0.05%	42
LIBS	Building material	0.1%	43
MW-LIBS	Cement	0.0047%	This work

The limit of detection (LoD) was calculated using the 3-sigma method.[38] The enhancing ability of MW-LIBS has been outlined in Fig. 7. The slope found using MW-LIBS data was ~4 times higher than the one from LIBS. The LoD was calculated for 100 shot accumulation and single shot measurements. The LoD for 100 shot accumulation was 47 ± 7 μg g^{-1} while for the single shot it was 170 ± 59 μg g^{-1}. The LoD found by MW-LIBS was compared with LIBS data from the same experiment. The corresponding value for 100 shot accumulation and a single shot with LIBS was 139 ± 23 μg g^{-1} and 168 ± 38 μg g^{-1}, respectively. The results show that the MW-LIBS yields a 3-fold improved limit of detection compared with LIBS. In addition to the superior chlorine LoD achieved, MW-LIBS offers ease of use and real-time detection. The LoD evaluated in this work represents a 10-fold improvement of the Cl detection limit reported in the literature as shown in Table 1.

4. Conclusion

Quantitative chlorine detection, *via* molecular emission, using a microwave assisted LIBS technique is reported. Chlorine detection with LIBS is also evaluated to show the benefit of using MW-LIBS over LIBS. Possible emission spectra of CaCl have been tested and the optimum emission spectrum of CaCl for developing the calibration curve has been identified. It was observed that the optimum signal of CaCl at around 617.9–621.5 nm was found at 500–1000 ns gate-delay and a gate-width of 300 μs. In addition, it was determined that a laser energy less than 7 mJ was not suitable for a proper calibration process. Using MW-LIBS, the LoD of chlorine is 47 ± 7 μg g^{-1}, and it presents a 3-fold improvement to that with LIBS. The LoD was obtained using a calibration curve of 10 cement samples, with different chlorine concentrations. The lowest chlorine concentration used was 800 μg g^{-1}. Although 800 μg g^{-1} is not very low, the recorded noise level was very low. The combination of the slope and the standard deviation, based on the 3-sigma method, yields the recorded 47 ± 7 μg g^{-1} LoD. The LoD evaluated in this work represents a 10-fold improvement to the Cl detection limit reported in the literature.

MW-LIBS offers a few advantages including usability at low laser energy and lifetime extension of the laser-induced-plasma. The former prevents significant sample damage and results in reliable averaging. The latter provides significant signal enhancement at a low noise level. This translates to an excellent LoD. MW-LIBS systems, however, require the use of microwave generators, waveguides and near field applicators. These additional elements add to the complexity of the detection setup, when compared to LIBS. Furthermore, a MW-LIBS setup, with a near field applicator, is not suitable for standoff applications.

Conflicts of interest

There are no conflicts to declare.

References

1 C. Gottlieb, T. Günther and G. Wilsch, *Spectrochim. Acta, Part B*, 2018, **142**, 74–84.
2 C. Gottlieb, S. Millar, T. Günther and G. Wilsch, *Spectrochim. Acta, Part B*, 2017, **132**, 43–49.
3 X. Xiao, S. Le Berre, K. C. Hartig, A. T. Motta and I. Jovanovic, *Spectrochim. Acta, Part B*, 2017, **130**, 67–74.
4 O. Forni, M. Gaft, M. J. Toplis, S. M. Clegg, S. Maurice, R. C. Wiens, N. Mangold, O. Gasnault, V. Sautter, S. Le Mouélic, P.-Y. Meslin, M. Nachon, R. E. McInroy, A. M. Ollila, A. Cousin, J. C. Bridges, N. L. Lanza and M. D. Dyar, *Geophys. Res. Lett.*, 2015, **42**, 1020–1028.
5 F. Weritz, D. Schaurich, A. Taffe and G. Wilsch, *Anal. Bioanal. Chem.*, 2006, **385**, 248–255.
6 C. Xiong, T. F. Zhang, D. Wang, Y. Lin, H. Qu, W. Chen, L. B. Luo, Y. B. Wang, L. Zheng and L. L. Fu, *Anal. Chim. Acta*, 2018, **1033**, 65–72.
7 D. S. Vogt, K. Rammelkamp, S. Schroder and H. W. Hubers, *Icarus*, 2018, **302**, 470–482.
8 S. Wu, T. Zhang, H. Tang, K. Wang, X. Yang and H. Li, *Anal. Methods*, 2015, **7**, 2425–2432.
9 N. Huber, S. Eschlböck-Fuchs, H. Scherndl, A. Freimund, J. Heitz and J. D. Pedarnig, *Appl. Surf. Sci.*, 2014, **302**, 280–285.
10 L. Dudragne, Ph. Adam and J. Amouroux, *Appl. Spectrosc.*, 1998, **52**, 1321–1327.
11 A. Khumaeni, T. Motonobu, A. Katsuaki, M. Masabumi and W. Ikuo, *Opt. Express*, 2013, **21**, 29755–29768.
12 C. Alvarez-Llamas, J. Pisonero and N. Bordel, *J. Anal. At. Spectrom.*, 2017, **32**, 162–166.

13 D. E. Anderson, B. L. Ehlmann, O. Forni, S. M. Clegg, A. Cousin, N. H. Thomas, J. Lasue, D. M. Delapp, R. E. McInroy, O. Gasnault, M. D. Dyar, S. Schroder, S. Maurice and R. C. Wiens, *J. Geophys. Res.*, 2017, **122**, 744–770.
14 K. Rammelkamp, D. S. Vogt, S. Schröder and H.-W. Hübers, presented in part at the *49th Lunar and Planetary Science Conference*, The Woodlands, Texas, LPI Contribution No. 2083, id. 1947, 2018.
15 T. A. Labutin, A. M. Popov, S. N. Raikov, S. M. Zaytsev, N. A. Labutina and N. B. Zorov, *J. Appl. Spectrosc.*, 2013, **80**, 315–318.
16 J. Serrano, J. Moros and J. J. Laserna, *Anal. Chem.*, 2015, **87**, 2794–2801.
17 C. Haisch, R. Niessner, O. I. Matveev, U. Panne and N. Omenetto, *Fresenius. J. Anal. Chem.*, 1996, **356**, 21–26.
18 A. De Giacomo and J. Hermann, *J. Phys. D: Appl. Phys.*, 2017, **50**, 17.
19 C. Álvarez, J. Pisonero and N. Bordel, *Spectrochim. Acta, Part B*, 2014, **100**, 123–128.
20 S. Yao, Y. Shen, K. Yin, G. Pan and J. Lu, *Energy Fuels*, 2015, **29**, 1257–1263.
21 A. H. Rezaei, M. H. Keshavarz, M. K. Tehrani and S. M. R. Darbani, *Laser Phys.*, 2018, **28**, 10.
22 L. B. Guo, Z. H. Zhu, J. M. Li, Y. Tang, S. S. Tang, Z. Q. Hao, X. Y. Li, Y. F. Lu and X. Y. Zeng, *Opt. Express*, 2018, **26**, 2634–2642.
23 C. R. Bhatt, B. Alfarraj, K. K. Ayyalasomayajula, C. Ghany, F. Y. Yueh and J. P. Singh, *Appl. Opt.*, 2015, **54**, 10264–10271.
24 M. Gaft, L. Nagli, N. Eliezer, Y. Groisman and O. Forni, *Spectrochim. Acta, Part B*, 2014, **98**, 39–47.
25 D. Vogt, K. Rammelkamp, S. Schröder and H.-W. Hübers, *presented in part at the LPSC 2017*, The Woodlands, USA, 2017.
26 A. A. Bol'shakov, X. Mao, J. J. González and R. E. Russo, *J. Anal. At. Spectrom.*, 2016, **31**, 119–134.
27 Y. Ikeda and R. Tsuruoka, *Appl. Opt.*, 2012, **51**, B183–B191.
28 A. Khumaeni, K. Akaoka, M. Miyabe and I. Wakaida, *Front. Phys.*, 2016, **11**, 114209.
29 Y. Tang, J. Li, Z. Hao, S. Tang, Z. Zhu, L. Guo, X. Li, X. Zeng, J. Duan and Y. Lu, *Opt. Express*, 2018, **26**, 12121–12130.
30 J. Viljanen, Z. Sun and Z. T. Alwahabi, *Spectrochim. Acta, Part B*, 2016, **118**, 29–36.
31 B. Kearton and Y. Mattley, *Nat. Photonics*, 2008, **2**, 537.
32 P. C. Efthimion, *Advances in Laser Assisted Microwave Plasma Spectroscopy (LAMPS)*, 2012.
33 Y. Liu, B. Bousquet, M. Baudelet and M. Richardson, *Spectrochim. Acta, Part B*, 2012, **73**, 89–92.
34 Y. Liu, M. Baudelet and M. Richardson, *J. Anal. At. Spectrom.*, 2010, **25**, 1316–1323.
35 A. Khumaeni, M. Miyabe, K. Akaoka and I. Wakaida, *J. Radioanal. Nucl. Chem.*, 2017, **311**, 77–84.
36 M. Tampo, M. Miyabe, K. Akaoka, M. Oba, H. Ohba, Y. Maruyama and I. Wakaida, *J. Anal. At. Spectrom.*, 2014, **29**, 886–892.
37 M. Wall, Z. W. Sun and Z. T. Alwahabi, *Opt. Express*, 2016, **24**, 1507–1517.
38 J. Viljanen, H. Zhao, Z. Zhang, J. Toivonen and Z. T. Alwahabi, *Spectrochim. Acta, Part B*, 2018, **149**, 76–83.
39 A. Iqbal, Z. Sun, M. Wall and Z. T. Alwahabi, *Spectrochim. Acta, Part B*, 2017, **136**, 16–22.
40 S. J. Chen, A. Iqbal, M. Wall, C. Fumeaux and Z. T. Alwahabi, *J. Anal. At. Spectrom.*, 2017, **32**, 1508–1518.
41 G. Wilsch, F. Weritz, D. Schaurich and H. Wiggenhauser, *Constr. Build. Mater.*, 2005, **19**, 724–730.
42 V. S. Burakov, V. V. Kiris and S. N. Raikov, *J. Appl. Spectrosc.*, 2007, **74**, 321–327.
43 F. Weritz, D. Schaurich and G. Wilsch, *Spectrochim. Acta, Part B*, 2007, **62**, 1504–1511.
44 C. D. Gehlen, E. Wiens, R. Noll, G. Wilsch and K. Reichling, *Spectrochim. Acta, Part B*, 2009, **64**, 1135–1140.